Journal of Thermal Analysis and Calorimetry, Vol. 89 (2007) 3, 675–680

EVALUATION OF COMPATIBILITY IN POLYMER BLEND SYSTEMS BY SIMULTANEOUS DSC-FTIR MEASUREMENT

S. Y. Jung, G. Zhang and H. Yoshida***

Department of Applied Chemistry, Graduate School of Urban Environmental Science, Tokyo Metropolitan University
Hachiouji, Tokyo 192-0397, Japan

The concept of crystallization dynamics method evaluating the miscibility of binary blend system including crystalline component was proposed. Three characteristic rates, nucleation, crystal growth rates (N^*, G^*) and growth rate of conformation (G_c^*) were used to evaluate the miscibility of PVDF/*at*-PMMA and PVDF/*iso*-PMMA by the simultaneous DSC-FTIR. N^*, G^* and G_c^* depended remarkably on both temperature and blend fraction (ϕ_{PMMA}) for PVDF/*at*-PMMA system, which indicated the miscible system. PVDF/*iso*-PMMA showed small ϕ_{PMMA} dependency of N^*, G^* and G_c^*, was estimated the immiscible system. The $\Delta T/T_m^0$ values, corresponding to Gibbs energy required to attend the constant G^* and G_c^*, evaluated from G^* and G_c^* showed the good linear relationships with different slope. The experimental results suggested that the concentration fluctuation existed in PVDF/*iso*-PMMA system.

Keywords: *concentration fluctuation, crystallization, DSC-FTIR, miscibility, polymer blend*

Introduction

Compatibility of simple binary liquid system is described by phase diagram, blend fraction (ϕ) – temperature (T) plot with co-existence (binodal) and spinodal curves shown in Fig. 1. Figures 1a and b show Gibbs energy change of mixing (ΔG_{mix}) at a given temperature T_1 (a) and phase diagram (b) of binary liquid system. At a given T_i, the minimums of ΔG_{mix}, the second derivative ($\partial^2\Delta G_{mix}/\partial\phi^2=0$) and the third derivative ($\partial^3\Delta G_{mix}/\partial\phi^3=0$) give binodal curve (solid curve), spinodal curve (dotted curve) and critical point (T_c and ϕ_c), respectively in Fig. 1b. Lower critical solution temperature (LCST) type binodal curve is observed for binary system having attractive interaction between blend components. Since the mixing of blend systems is carried out at T_{mix} in the molten state or the super-cooled liquid state, the relationship between the binodal curve and the phase transitions, such as melting and glass transitions, become important to discuss the compatibility of binary blend system including solid component. The binodal curve should exist at higher temperature than the melting temperature for the miscible binary systems as shown in Fig. 1c, because the blend system is the mixed phase at T_{mix}. If the binodal curve exists close to the melting temperature of crystalline component, the miscibility depends on the thermal

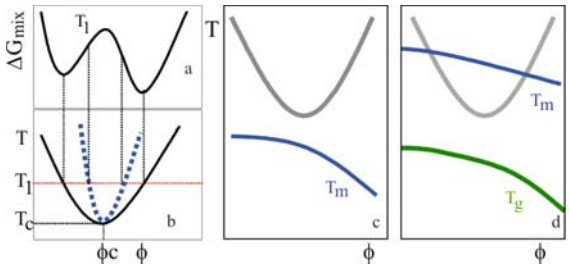

Fig. 1 Schematic drawings of phase diagram for binary liquid system (a, b) and binary system including crystalline component (c, d). Gibbs energy difference of mixing at a given temperature (a) and corresponding phase diagram (b)

history of system. For instance, the system is miscible, if T_{mix} is in the temperature range between the binodal curve and the melting temperature. However, the system is immiscible, if T_{mix} is above the binodal curve. For the immiscible binary system, the binodal curve is overlap with the melting temperature (T_m) curve or closed with the glass transition temperature (T_g) curve as shown in Fig. 1d.

Compatibility of organic materials including polymers is essentially described by thermodynamics, such as Huggins–Flory [1, 2] and Simha theory [3] for universal binary systems, and Nishi–Wang equation [4] for blend system with crystalline polymer. For polymer–polymer blend system, the attractive interaction between blend components is

* Present address: School of Chemical Engineering and Environment, Beijing Institute of Technology, Beijing 100081, China
** Author for correspondence: yoshida-hirohisa@tmu.ac.jp

1388–6150/$20.00

Akadémiai Kiadó, Budapest, Hungary
Springer, Dordrecht, The Netherlands

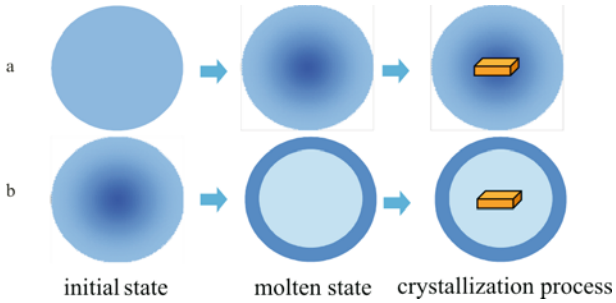

Fig. 2 Schematic drawings of phase separation and crystallization in the a – miscible and b – immiscible system

necessary to form the miscible system because the combinatorial entropy becomes scarcely contributing for the mixing. With increasing molecular mass of components, however, blend systems become difficult approaching the equilibrium state due to the lower diffusion coefficient of molecules. We have proposed 'crystallization dynamics method' to evaluate the miscibility of binary polymer blend systems containing crystalline component [5]. In this method, the kinetic process approaching the equilibrium or the quasi-equilibrium state is affected by the mixing state of blend components at the super-cooled liquid state of system as shown in Fig. 2. When the miscible system a is heated in the molten state which is the lower temperature region than the binodal curve, the system is in the one phase. The system is cooled to the crystallization temperature region, the crystallization occurs in the miscible state. The nucleation rate (N^*), crystal growth rate (G^*) and surface energy of crystallite (σ) depend on blend fraction for the miscible systems as shown in Fig. 2a. In the case of immiscible system, the phase separation occurs in the molten state, the crystallization occurs in the one phase including higher content of crystalline component, therefore N^*, G^* and σ are independent on blend fraction for the immiscible systems as shown in Fig. 2b.

We have reported the miscibility of polymer blend using the crystallization dynamics method for poly(vinylidene fluoride) and poly(methyl methacrylate) (PVDF/PMMA) system [6], PVDF/poly(alkyl methacrylate) systems [7], nylon 66/nylon 48 system [8, 9], syndiotactic polystyrene/atactic polystyrene system [10], nylon 66/nylon 6 system [11] and di-block copolymer/homopolymer systems [12, 13]. In this study, the compatibility of polymer blend systems were investigated by crystallization dynamics method using the simultaneous differential scanning calorimeter and Fourier transform infrared spectrometer (DSC-FTIR).

Experimental

Samples

PVDF supplied by Kureha Chemical Co. Ltd. (M_n; $26.0 \cdot 10^5$, T_m of α-form; 453 K), atactic poly(methyl methacrylate) (*at*-PMMA, M_n; $1.5 \cdot 10^5$, M_n/M_w; 1.5, [I]:[S]:[H]=0.13:0.43:0.44) and isotactic PMMA (*iso*-PMMA, M_n; $1.6 \cdot 10^5$, M_n/M_w; 1.7, [I]:[S]:[H]=0.93:0.03:0.04) were used for PVDF/PMMA blends. PVDF and PMMA were dissolved in N,N-dimethylacetamide at room temperature, blend samples were obtained by solvent casting. The blend fraction was indicated by mass fraction of PMMA (ϕ_{PMMA}). Blend samples were pressed at 473 K and were quenched to ice water. Blend sample film sandwiched with two thin KBr dishes and cramped in an aluminum sample vessel was used for DSC-FTIR measurement. Sample mass used was about 1.5 mg.

Instruments

The simultaneous DSC-FTIR measurement was carried out by setting the simultaneous DSC instrument [14] on the JASCO FTIR 620 with MCT (Mercury Cadmium Telluride) detector in the wavenumber range between 650 and 4000 cm^{-1}. The accumulation of one spectrum and the wavelength resolution were 2 times and 2 cm^{-1}, respectively. Under this condition, the time resolution of FTIR spectra was 15 s. The scanning velocity and the time resolution of DSC were 5 K min^{-1} and 1.0 s, respectively. The sample was heated to 473 K and maintained for 5 min, then quenched to a predetermined crystallization temperature (T_c). The heat of crystallization at T_c was measured until the crystallization was completed. During isothermal crystallization, DSC exothermal and FTIR spectra were recorded simultaneously. Temperature variation during crystallization was at most ±0.2 K. Isothermal crystallization was carried out at various T_c. After crystallization, samples were quenched under 373 K and the melting temperature (T_m) and the melting enthalpy (ΔH_m) were measured 5 K min^{-1} on heating. The equilibrium melting point (T_m^0) of sample was estimated by extrapolating the relationship between T_m and T_c according to Hoffman and Weeks [15].

Results and discussion

Two characteristic times t_N and $t_{1/2}$ were evaluated from DSC curve during the isothermal crystallization. The time required from the isothermal condition was established (t_0) to the starting time of exothermic peak

(t_S) and the time required to produce a half of crystallite (t_H) from t_S were indicated the nucleation time (t_N=t_S–t_0) and the half time of crystallization ($t_{1/2}$=t_H–t_S), respectively. The reciprocal of t_N and $t_{1/2}$ were used as the nucleation rate (N^*=1/t_N) and the crystal growth rate (G^*=1/$t_{1/2}$), respectively. According to Lauritzen and Hoffman [16], the temperature dependency of G^* is described as follows.

$$G^* = G_0^* \exp\left(\frac{-\Delta E}{RT} - \frac{KT_m}{RT\Delta T}\right) \quad (1)$$

$$K = nbT_m\sigma/\Delta H_m^2 \quad (2)$$

$$\sigma = \sigma_s^2\sigma_e \quad (3)$$

where, ΔE, ΔT, G_0^*, R, n, b, ΔH_m, σ_s and σ_e indicate the activation energy of migration through the nucleus melt interface, the crystallization constant that is independent of temperature, the degree of supercooling (ΔT=T_m–T_c), the pre-exponential factor, the gas constant, the constant depending on the crystallization regime, the length of stem, the heat of melting, the lateral surface free energy and the fold surface energy of crystallite, respectively. According to Turbull and Fisher [17], the temperature dependency of N^* is given by the following equation.

$$N^* = N_0^* \exp\left(-\frac{ST_m^2}{T\Delta T^2}\right) \quad (4)$$

$$S = A\left(\frac{2\sigma}{R\Delta H_m^2} - \frac{T\log(V_a)\sigma_e}{\Delta H_m^2}\right) \quad (5)$$

where, N_0^*, A and V_a indicated the nucleation constant that is independent of temperature, a constant that depends on both nucleation and crystal growth processes and the volume fraction of amorphous component, respectively. Equations (2) and (5) indicated that K and S were the parameter of surface free energy of crystallite obtained from G^* and N^*, respectively.

From DSC results during the isothermal crystallization, G^* and N^* were determined at each T_c. G^* and N^* are plotted *vs.* ΔT for PVDF/*at*-PMMA and PVDF/*iso*-PMMA in Figs 3 and 4, respectively. ΔT was determined from the corresponding T_m^0 for each ϕ_{PMMA}. For PVDF/*at*-PMMA system, both G^* and N^* depended on T_c and ϕ_{PMMA}, and G^* showed the similar ϕ_{PMMA} dependency of N^*. The results shown in Fig. 3 suggested that the nucleation and crystal growth process became slower with the increase of ϕ_{PMMA} for PVDF/*at*-PMMA system. PVDF/*iso*-PMMA showed the T_c dependency of G^* and N^*, however, both G^* and N^* slightly depended on ϕ_{PMMA}. In order to clarify the ϕ_{PMMA} dependency of G^* and N^*, the ΔT value at constant G^* and N^* were evaluated for each ϕ_{PMMA} from Figs 3 and 4.

At the nucleation process from the molten state, Gibbs energy difference between the liquid state and the crystalline state (ΔG) which is the driving force of nucleation is written by the following equation.

$$\Delta G = \frac{\Delta H_m \Delta T}{T_m} \quad (6)$$

The ΔT values were obtained from Figs 3 and 4 at 0.005 s^{-1} of G^* and N^*. $\Delta T/T_m^0$ indicated ΔG required to attain the constant G^* or N^*. The relationship between $\Delta T/T_m^0$ and ϕ_{PMMA} were shown in Fig. 5 obtained from G^* (a) and N^* (b). Although G^* and N^* were evaluated from the different experimental quantities, both $\Delta T/T_m^0$ values obtained from G^* and N^* showed a good agreement.

For the miscible PVDF/PMMA system, the attractive interaction worked between hydrogen of PVDF and carbonyl oxygen of PMMA. For the crystallization of polymer, the rate-determining process is the diffusion of polymer molecules through the interface between the nuclei or the growth surface

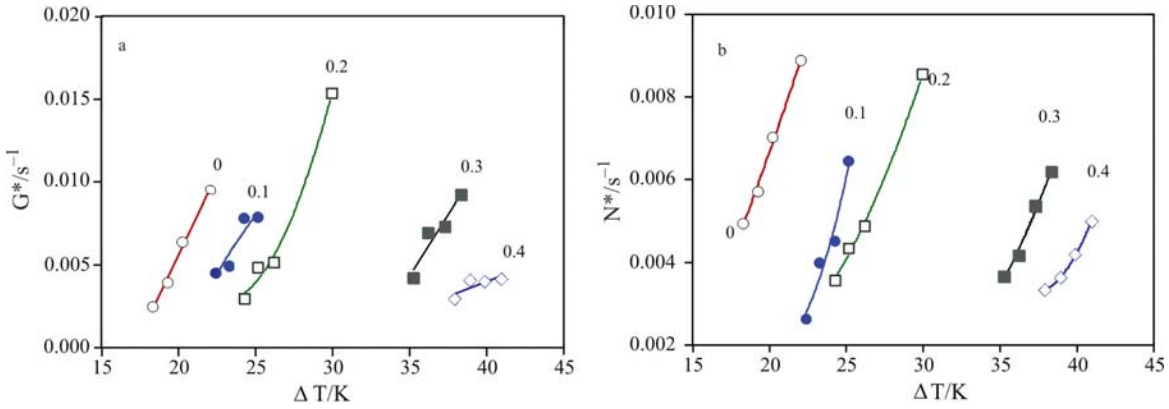

Fig. 3 Relationship between a – crystal growth rate (G^*), b – nucleation rate (N^*) and degree of super-cooling (ΔT=T_m–T_c) for PVDF/*at*-PMMA system

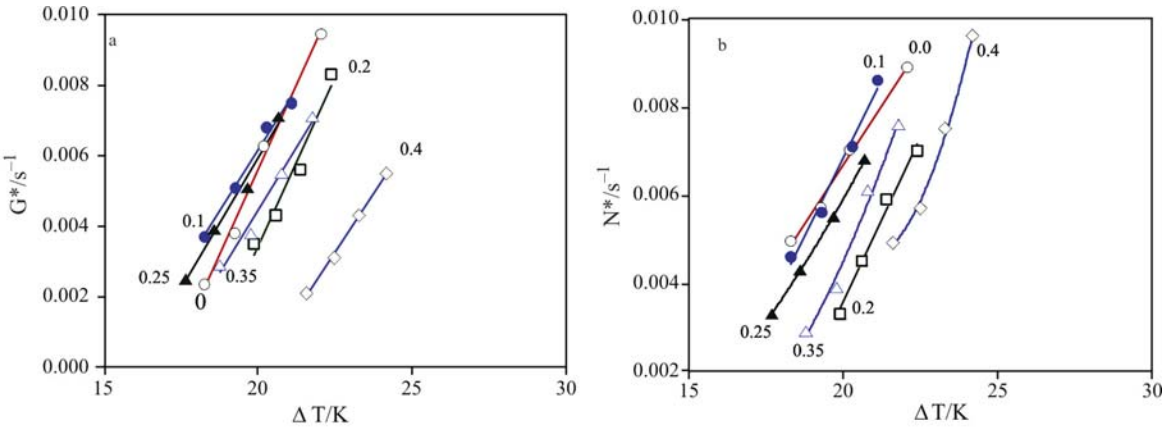

Fig. 4 Relationship between a – crystal growth rate (G^*), b – nucleation rate (N^*) and degree of super-cooling ($\Delta T=T_m-T_c$) for PVDF/*iso*-PMMA system

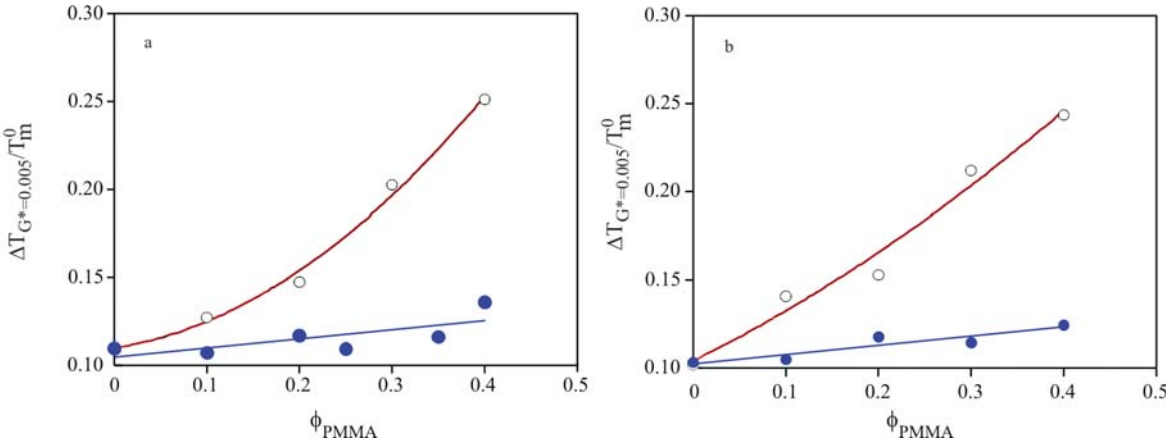

Fig. 5 Changes of Gibbs energy difference parameter $\Delta T/T_m^0$ evaluated a – at G^*=0.005 s^{-1}, b – at N^*=0.005 s^{-1} as a function of blend faction (ϕ_{PMMA}) for PVDF/*at*-PMMA and PVDF/*iso*-PMMA systems

and the molten state. During the crystallization of PVDF in the miscible PVDF/PMMA blend system, PVDF molecules diffused among PMMA molecules which interacted attractively with PVDF. The diffusion of PVDF depended on the interaction strength and the number of PMMA surrounding PVDF. Therefore, both G^* and N^* delayed with the increase of ϕ_{PMMA} in the miscible PVDF/PMMA system, and then ΔG required to attain the constant G^* and N^* increased with the ϕ_{PMMA}. The results shown in Fig. 5 suggested that PVDF/*at*-PMMA system was the miscible system. The relationship between ΔG and ϕ_{PMMA} for PVDF/*iso*-PMMA was also linear, however, the slope of linear relationship was smaller than that of PVDF/*at*-PMMA. This result suggested that PVDF/*iso*-PMMA was the immiscible system or the attractive interaction between PVDF and *iso*-PMMA was smaller than that in PVDF/*at*-PMMA.

Not only for DSC exothermic peak but also IR spectrum changes were obtained during the iso-thermal crystallization by DSC-FTIR. The IR bands at 795 and 763 cm^{-1} are assigned to rocking mode of CH_2 and bending mode of CF_2, respectively [18]. Both bands correspond to the TGTG' conformation, which is a unique conformation of α-form of PVDF crystal. Changes of TGTG' conformation ($X_{TGTG'}$) was evaluated from the changes of IR absorbance at 763 cm^{-1} during isothermal crystallization. The change of TGTG' conformation ($X_{TGTG'}$) was defined to be the fraction relative absorbance at 763 cm^{-1}.

$$X_{TGTG'} = (At - At_0)/(At_{max} - At_0) \qquad (7)$$

where At, At_0 and At_{max} indicate the absorbance at 763 cm^{-1} at time t, the initial time t_0 and the final time of crystallization t_{max}, respectively. Two characteristic half time of conformational ordering was evaluated from the absorbance change at 763 cm^{-1}. The time required to approach 50% of $X_{TGTG'}$ from t_0 was determined as $t_{TGTG'}$, respectively. The reciprocal $t_{TGTG'}$ was employed as the growth rate of TGTG' conformation ($G_c^*=1/t_{TGTG'}$), respectively.

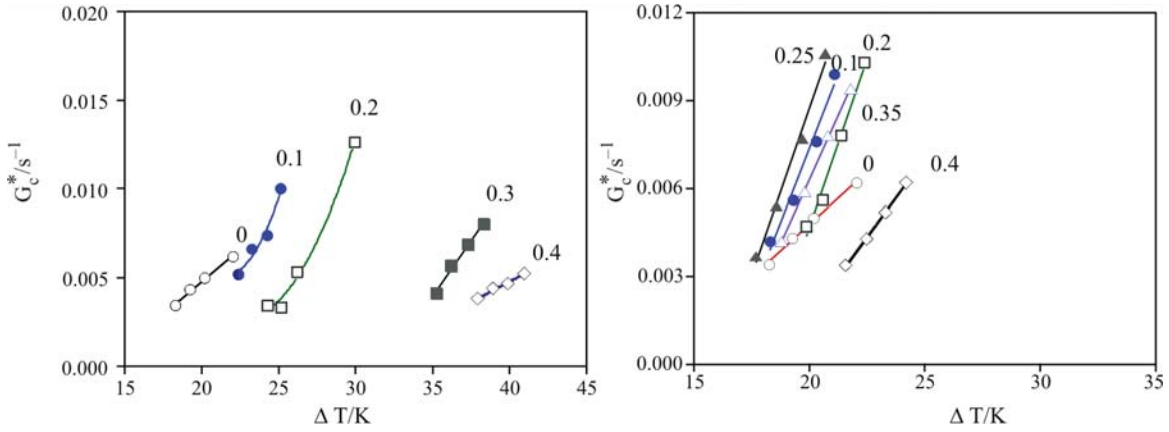

Fig. 6 Relationship between conformational growth rate (G^*) and degree of super-cooling ($\Delta T=T_m-T_c$) for a – PVDF/*at*-PMMA system and b – PVDF/*iso*-PMMA system

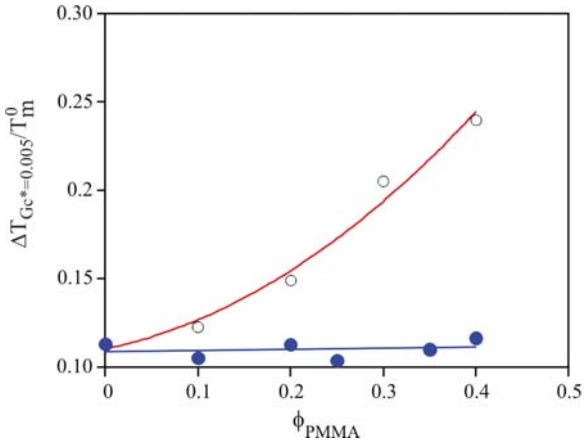

Fig. 7 Changes of Gibbs energy difference parameter $\Delta T/T_m^0$ evaluated at G_c^*=0.005 s^{-1} as a function of blend faction (ϕ_{PMMA}) for PVDF/*at*-PMMA and PVDF/*iso*-PMMA systems

Figure 6 shows the relationship between G_c^* and ΔT for PVDF/*at*-PMMA (a) and PVDF/*iso*-PMMA (b) with various ϕ_{PMMA}. PVDF/*at*-PMMA system showed the similar ϕ_{PMMA} dependency of G_c^* with G^* shown in Fig. 3a, however, the ϕ_{PMMA} dependency of G_c^* for PVDF/*iso*-PMMA system differed from that of G^* shown in Fig. 3b. The ΔT values at a constant G_c^* (0.005 s^{-1}) were obtained for each ϕ_{PMMA} from Fig. 6. Figure 7 shows the relationship between $\Delta T/T_m^0$ and ϕ_{PMMA} obtained from G_c^* for PVDF/*at*-PMMA and PVDF/*iso*-PMMA. Both systems showed the similar tendency shown in Fig. 5a.

Figure 8 shows the relationship between the $\Delta T/T_m^0$ values obtained from G^* and G_c^*. Both blend systems showed the linear relationships with different slopes. The slope values were 1 and 0.35 for PVDF/*at*-PMMA and PVDF/*iso*-PMMA, respectively. G^* and G_c^* evaluated from the results of the simultaneous DSC-FTIR measurement. In polymer crystallization from the molten state, the rate-determining process is the diffusion of molecules to crystal growth surface. If the diffusion process of polymer is described by the repetitation model [19], the diffusion distance is almost the same with the radius of gyration of polymer molecules (R_g):

$$R_g = \frac{1}{\sqrt{6}} N^{1/2} l \tag{8}$$

where, N and l indicate number and length of repeating unit, respectively. The R_g value evaluated from molecular mass of PVDF was 20 nm according to Eq. (5). That is to say, G^* is influenced by the average blend fraction in the area with a radius of 20 nm. On the other hand, a conformational ordering of a polymer chain occurs as intermolecular phenomena. Polymer-polymer interactions may affect the formation of chain conformations. Specific interactions are very sensitive to the distance between the interacting groups. Since the interaction between

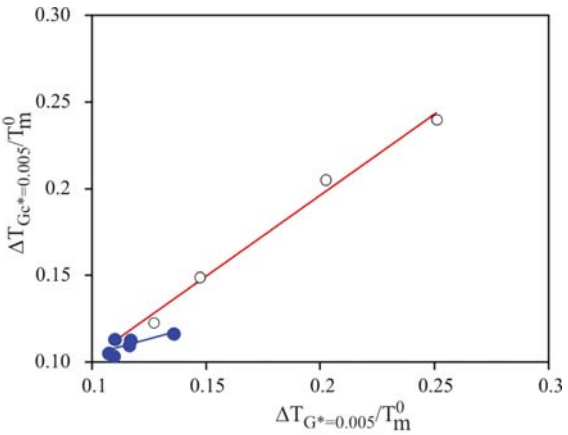

Fig. 8 Relationship between two Gibbs energy difference parameters $\Delta T/T_m^0$ evaluated at G_c^*=0.005 s^{-1} and G_c^*=0.005 s^{-1} for PVDF/*at*-PMMA and PVDF/*iso*-PMMA systems

PVDF and PMMA is the electrostatic interaction, the electrostatic interaction works between the first closest neighbors, therefore, the distance evaluated from the interaction between two-polymer chains is expected in the order of 1 nm. G_c^* of TGTG' conformation, obtained by FTIR, reflects the average blend fraction in the area within a radius of 1 nm. Therefore, the blend fraction in the different spaces in PVDF/*at*-PMMA system was same, in the other word, PVDF and *at*-PMMA are miscible in molecular level. On the other hand, PVDF/*iso*-PMMA system indicated that the blend fraction in the space with 1 nm differed from that in the space with 20 nm, this was to say, the concentration fluctuation existed in PVDF/*iso*-PMMA system.

References

1 M. L. Huggins, J. Chem. Phys., 9 (1941) 440.
2 P. J. Flory, J. Chem. Phys., 9 (1941) 660.
3 R. K. Jain and R. Simha, Macromolecules, 13 (1980) 1501.
4 T. Nishi, T. T. Wang and T. K. Kwei, Macromolecules, 8 (1975) 227.
5 H. Sasaki, G. Bara and H. Yoshida, Polymer, 25 (1995) 4805.
6 H. Yoshida, J. Thermal Anal., 49 (1997) 101.
7 H. Yoshida, G. Z. Zhang, T. Kitamura and T. Kawai, J. Therm. Anal. Cal., 64 (2001) 577.
8 G. Z. Zhang, H. Yoshida, T. Watanabe and T. Kawai, Polymer J., 35 (2003) 188.
9 G. Z. Zhang, H. Yoshida and T. Kawai, Thermochim. Acta, 416 (2004) 79.
10 T. Watanabe, G. Z. Zhang, H. Yoshida and T. Kawai, J. Therm. Anal. Cal., 72 (2003) 57.
11 G. Z. Zhang, C. Liu and H. Yoshida, J. Therm. Anal. Cal., 81 (2006) 707.
12 S. Y. Jung, T. Yamada, H. Yoshida and T. Iyoda, J. Therm. Anal. Cal., 81 (2005) 563.
13 S. Y. Jung and H. Yoshida, J. Therm. Anal. Cal., 81 (2006) 719.
14 H. Yoshida, R. Kinoshita and Y. Teramoto, Thermochim. Acta, 264 (1995) 173.
15 J. D. Hoffman and J. J. Weeks, J. Res. Nat. Bur. Stand. (H), 66 (1962) 13.
16 J. I. Lauritzen and J. D. Hoffman, J. Appl. Phys., 44 (1073) 4340.
17 D. Turnbull and J. C. Fisher, J. Chem. Phys., 17 (1949) 71.
18 J. S. Noland, N. N. C. Hsu, R. Saxon and J. M. Schmitt, ACS Adv. Chem. 99 (1971).
19 P-G. De Gennes,'Scaling Concepts in Polymer Physics', Cornell University Press (1979), p. 224.

DOI: 10.1007/s10973-006-7954-y